3-1-2021

Application of short-time stochastic subspace identification to estimate bridge frequencies from a traversing vehicle

Nan Jin

Y. B. Yang

Elias G. Dimitrakopoulos

Themelina S. Paraskeva
Edith Cowan University

Lambros S. Katafygiotis

10.1016/j.engstruct.2020.111688

This is an author's accepted manuscript of: Jin, N., Yang, Y. B., Dimitrakopoulos, E. G., Paraskeva, T. S., & Katafygiotis, L. S. (2021). Application of short-time stochastic subspace identification to estimate bridge frequencies from a traversing vehicle. *Engineering Structures, 230*, article 111688. https://doi.org/10.1016/j.engstruct.2020.111688

Highlights

- The study establishes a framework to identify bridge frequencies from a moving test vehicle
- Gives theoretical support to eliminate the negative effect of road roughness from the identification results
- The approach adopts a dimensionless description to cope with the time-varying nature of VBI
- The method is verified via numerical experiments with both SDOF and MDOF vehicles
- The method allows identifying bridge frequencies using test vehicles with practical speeds even considering poor road surface

Application of Short-time Stochastic Subspace Identification to Estimate Bridge Frequencies from a Traversing Vehicle

Nan JIN[1], Y. B. YANG[2,3], Elias G. DIMITRAKOPOULOS[1*]
Themelina S. PARASKEVA[4], Lambros S. KATAFYGIOTIS[1],

[1]Department of Civil and Environmental Engineering,
Hong Kong University of Science and Technology, Clear Water Bay, Kowloon Hong Kong

[2]School of Civil Engineering, Chongqing University, Chongqing 400045, China

[3]Department of Construction Engineering
National Yunlin University of Science and Technology, Yunlin, Taiwan

[4]School of Engineering
Edith Cowan University, Joondalup WA 6027, Australia

*** Correspondence:**
Elias G. Dimitrakopoulos
ilias@ust.hk

Keywords: vehicle-bridge interaction, subspace identification, dimensionless description, indirect identification

Abstract

This study establishes a short-time stochastic subspace identification (ST-SSI) framework to estimate bridge frequencies by processing the dynamic response of a traversing vehicle. The formulation uses a dimensionless description of the response that simplifies the vehicle-bridge interaction (VBI) problem and brings forward the minimum number of parameters required for the identification. With the aid of

the dimensionless parameters the analysis manages to successfully apply ST-SSI despite the time-varying nature of the VBI system. Further, the proposed approach eliminates the adverse effect of the road surface roughness using a transformed residual vehicle response obtained from two traverses of a vehicle at different speeds over the bridge. The study verifies the proposed ST-SSI approach numerically: it first performs the dynamic VBI simulations to obtain the response of the vehicle, and then applies the proposed ST-SSI method, assuming the dynamic characteristics of the vehicle are available. The numerical experiments concern both a sprung mass model and a more realistic multi-degree-of-freedom (MDOF) vehicle model traversing a simply supported bridge. The results show that the proposed approach succeeds in identifying the first two bridge frequencies for test-vehicle speeds much higher (e.g., 10m/s = 36km/h and 20m/s = 72km/h) than previously considered, even in the presence of high levels of road surface roughness.

1 Introduction

The natural frequencies of a bridge may contain vital information about its health and are therefore essential to monitor. To estimate modal frequencies of a bridge, traditional techniques process data of its response measured using sensors installed on-site (Chatzi & Spiridonakos, 2015; Ferrari et al., 2016; Goi & Kim, 2016). These identification techniques are well-established but entail considerable effort and costs.

Over the past decade, there has been growing interest in extracting the dynamic properties of a bridge from the response of traversing vehicles (Yang et al., 2004a; Yang & Yang, 2018). The vehicle and the supporting bridge interact as the vehicle passes, forming a coupled system. It is thus feasible to extract information about the bridge by processing the response of the vehicle (Yang et al., 2004a). This indirect approach uses traversing vehicles both to excite a bridge and to collect information about the bridge. Compared with conventional identification methods, the indirect methods are more economical, portable, time-saving, and more easily implementable.

A first indirect approach is to use fast Fourier transform (FFT) of the acceleration response of the vehicle to identify bridge frequencies. This has been attempted in analytical studies (Yang et al., 2004a), numerical simulations (McGetrick et al., 2009), laboratory experiments (Urushadze & Yau, 2017) and field tests (Siringoringo & Fujino, 2012; Yang et al., 2013a; Yang et al., 2020). This method faces several challenges: (a) vehicle frequencies may dominate over bridge frequencies in the response spectrum of the vehicle; similarly, (b) road roughness often blurs the existence of bridge frequencies in the spectrum; and (c) higher modal frequencies of the bridge are usually hidden as they are not excited sufficiently. To suppress vehicle frequencies, Yang et al. (2013b) proposed the use of singular spectrum analysis with a band-pass filter. To deal with the blurring effect of the road roughness conditions (RRCs), Chang et al. (2010) employed a sequence of vehicles and increased speeds of the vehicles to amplify bridge vibration. Yang et al. (2012) and Kim et al. (2016) developed a residual Fourier spectrum, using the difference between the response of two connected vehicles to mitigate the effect of irregularity. To amplify higher bridge modes and facilitate their identification, Yang and Chang (2009) processed the vehicle response using empirical mode decomposition. This procedure also suppressed the fundamental bridge frequency, which prompted Yang and Lee (2018) to improve this algorithm by increasing vehicle damping.

Alternatively, bridge frequencies can be extracted from the vehicle response by means of general-purpose system identification techniques, e.g., stochastic subspace identification (SSI). Yang & Chen (2015) employed SSI to identify the frequencies of a simply supported beam from the response of a sprung mass vehicle model. The numerical results showed that assuming the basic parameters, vibration and path of the test-vehicle known, the SSI method could identify bridge modal frequencies from the vehicle response. Two pre-requisites for successful identification were: (i) there must be at least good RRC, and (ii) the vehicle must have a slow speed to conceal the time-varying nature of the VBI system. Jin et al. (2017; 2018) verified the SSI method with a more realistic VBI model, concluding that on-going traffic may be beneficial to the identification of higher-mode bridge frequencies. However, this SSI approach entailed considerable computational cost related to the repetitive calculations of pseudo-inverse matrices. Li et al. (2019) suggested using two vehicles, one

slowly traversing the bridge and one additional stationary vehicle serving as a reference sensor on the bridge. With the aid of the two vehicles they identified both frequencies and mode shapes of the bridge through numerical simulations and laboratory experiments.

This study deploys a short-time stochastic subspace identification (ST-SSI) technique to estimate bridge frequencies by processing the data from a traversing test-vehicle. The proposed ST-SSI method requires only the vibration response and dynamic properties of a test-vehicle, and controlling the speeds of the test-vehicle for two traverses over the bridge. The transformed residual response from two runs efficiently eliminates the adverse effect of road roughness from the output signal for the ST-SSI method. The proposed framework relies on a dimensionless description (Stoura & Dimitrakopoulos, 2019) that elucidates the underlying physical mechanisms of VBI. The dimensionless parameters simplify both the VBI problem and the inverse identification problem. Then effectively interprets the feasibility, as well as the limitations of applying the ST-SSI method to the time-varying VBI system.

The motivation for the present study stems from the need to extend the applicability of indirect identification in the direction of more realistic RRCs and more practical speeds of test-vehicle. The present analysis: (i) gives theoretical support to eliminate the negative effect of road roughness by removing related terms from the output signal for the ST-SSI method; (ii) explains the feasibility and the limitations of applying the ST-SSI method to a time-varying VBI system; and (iii) explores the possibility of using a traversing test-vehicle with practical speeds for the ST-SSI method.

2 Methodology

2.1 A brief review of short-time stochastic subspace identification

A widely-used method of system identification for a linear time-invariant (LTI) system in the state space (Katayama, 2006) is stochastic subspace identification (SSI). Consider a general output-only dynamic system with output (vector) $\mathbf{Y}_k$. One can describe the time-discrete LTI system with two equations

$$\mathbf{X}_{k+1} = \mathbf{A}\mathbf{X}_k + \mathbf{w}_k \tag{1}$$

$$\mathbf{Y}_k = \mathbf{C}\mathbf{X}_k + \mathbf{v}_k \tag{2}$$

where $\mathbf{X}_k$ is the state vector; $\mathbf{A}$ and $\mathbf{C}$ denote the time-invariant system matrices; $\mathbf{w}_k$ and $\mathbf{v}_k$ are system noise and measurement noise, respectively, which are modeled as zero-mean white noise. SSI allows to estimate the time-invariant system matrices $\mathbf{A}$ and $\mathbf{C}$ from the assumed measured output signal $\mathbf{Y}_k$.

Contrary to SSI, short-time stochastic subspace identification (ST-SSI) method is applicable to time-varying systems, provided that the time-variation (of their dynamic properties) is much slower than the dynamics of the system during the defined time-interval (Ohsumi & Kawano, 2002; Marchesiello et al., 2009). In other words, ST-SSI allows system matrices $\mathbf{A}$ and $\mathbf{C}$ in Eqs.(1) and (2) to be time-varying. A particular goal of the present study is to formulate the identification — of bridge frequencies from the response of a traversing vehicle — problem in a suitable form for ST-SSI, and to identify the system matrix $\mathbf{A}$ (see e.g., Eq. 1) that contains solely the dynamic properties of the bridge by processing the data from a traversing vehicle (vector $\mathbf{Y}_k$ in Eq. 2). In this context, the study also investigates, with the aid of a dimensionless description of the VBI problem, the range of application of the proposed approach.

2.2 Formulation of VBI system with dimensionless terms

Figure 1(a) shows the model of a simple vehicle-bridge system. The bridge is a simply supported Euler-Bernoulli beam of uniform cross-section with N degrees of freedom (DOFs). As a first approach, the vehicle is a single DOF (SDOF) mass m^{V}, moving with speed v and supported by a spring of stiffness k_c and dashpot of damping coefficient c_c. One way to state the equations of motion (EOM) of the coupled vehicle-bridge system (as Fig. 1b) (Zeng et al., 2016; Paraskeva et al., 2017) is

$$m^{\mathrm{V}} \frac{d^2}{dt^2} \tilde{u}^{\mathrm{V}}(t) = \tilde{\lambda}_N(t) \tag{3}$$

for the sprung mass, and

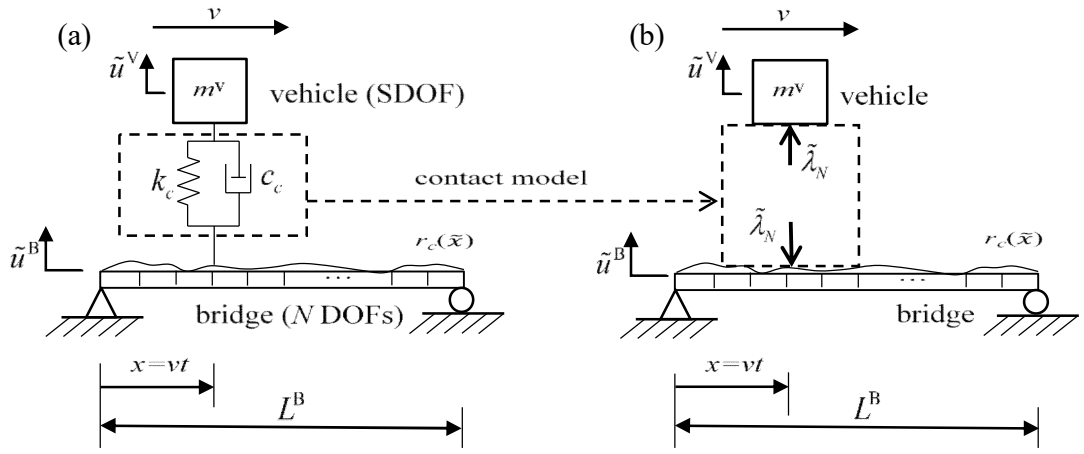

Figure 1. A simple vehicle-bridge interaction system

$$\mathbf{M}^{\mathrm{B}}\frac{d^2}{dt^2}\tilde{\mathbf{u}}^{\mathrm{B}}(t)+\mathbf{K}^{\mathrm{B}}\tilde{\mathbf{u}}^{\mathrm{B}}(t)+\mathbf{C}^{\mathrm{B}}\frac{d}{dt}\tilde{\mathbf{u}}^{\mathrm{B}}(t)+\mathbf{W}_N^{\mathrm{B}}(x)\tilde{\lambda}_N(t)=\mathbf{F}_G^{\mathrm{V}} \tag{4}$$

for the bridge, where $\mathbf{M}^{\mathrm{B}}$, $\mathbf{K}^{\mathrm{B}}$ and $\mathbf{C}^{\mathrm{B}}$ are the mass, stiffness and damping matrices of the bridge; $\tilde{u}^{\mathrm{V}}(t)$ and $\tilde{\mathbf{u}}^{\mathrm{B}}(t)$ are the response displacement of the vehicle and the bridge, respectively; $\mathbf{F}_G^{\mathrm{V}}=\mathbf{W}_N^{\mathrm{B}}(\tilde{x})m^{\mathrm{V}}g$ is the external force including the gravity of the vehicle; and $\mathbf{W}_N^{\mathrm{B}}(\tilde{x})$ defines the position of the contact force $\tilde{\lambda}_N(t)$ between vehicle and bridge, with the aid of conventional shape functions (Appendix A.1), equal with

$$\begin{aligned}\tilde{\lambda}_N(t)&=k_c\left(-\tilde{u}^{\mathrm{V}}(t)+\mathbf{W}_N^{\mathrm{B}}(\tilde{x})^{\mathrm{T}}\tilde{\mathbf{u}}^{\mathrm{B}}(t)+r_c(\tilde{x})\right)\\&+c_c\left(-\frac{d}{dt}\tilde{u}^{\mathrm{V}}(t)+\mathbf{W}_N^{\mathrm{B}}(x)^{\mathrm{T}}\frac{d}{dt}\mathbf{u}^{\mathrm{B}}(t)+v\frac{d}{d\tilde{x}}\mathbf{W}_N^{\mathrm{B}}(x)^{\mathrm{T}}\mathbf{u}^{\mathrm{B}}(t)+v\frac{d}{dx}r_c(x)\right)\end{aligned} \tag{5}$$

where $r_c(x)$ denotes the road roughness profile.

For the needs of the proposed ST-SSI method, we cast the interaction relationship between vehicle and bridge response (i.e., contact force $\tilde{\lambda}_N(t)$ Eq. 5) into the form of Eq. (2), and the EOM of the bridge (Eq. 4) into the form of Eq.(1). In addition, since Eqs. (4) and (5) involve a large number of parameters, we simplify the VBI problem and the subsequent identification problem, writing the contact force $\tilde{\lambda}_N(t)$ (Eq. 5) and the EOM of the bridge (Eq. 4) subsystem using dimensionless terms (Stoura &

Dimitrakopoulos, 2019). Specifically, multiplying Eq.(5) with $1/m^{\mathrm{V}}\left(\omega^{\mathrm{V}}\right)^2 L^{\mathrm{B}}$, and using the dimensionless time $\tau=\omega^{\mathrm{V}}t$ gives

$$\lambda_N(\tau)+u^{\mathrm{V}}+2\zeta^{\mathrm{V}}\dot{u}^{\mathrm{V}}=\left(\mathbf{W}_N^{\mathrm{B}}(x)^{\mathrm{T}}+\frac{2\nu\zeta^{\mathrm{V}}}{\omega^{\mathrm{V}}L^{\mathrm{B}}}\mathbf{W}_N^{\mathrm{B}}(x)'^{\mathrm{T}}\right)\mathbf{u}^{\mathrm{B}}+2\zeta^{\mathrm{V}}\mathbf{W}_N^{\mathrm{B}}(x)^{\mathrm{T}}\mathbf{u}^{\mathrm{B}}+R(x)+\frac{2\nu\zeta^{\mathrm{V}}}{\omega^{\mathrm{V}}L^{\mathrm{B}}}R(x)' \quad (6)$$

where $\lambda_N(\tau)$ is the dimensionless contact force; ω^{V} is the frequency of the vehicle; $u^{\mathrm{V}}=\tilde{u}^{\mathrm{V}}(\tau)/L^{\mathrm{B}}$ is the dimensionless vehicle response; $\mathbf{u}^{\mathrm{B}}=\tilde{\mathbf{u}}^{\mathrm{B}}(\tau)/L^{\mathrm{B}}$ is the dimensionless bridge response; $x=\tilde{x}/L^{\mathrm{B}}$ is the dimensionless position of the vehicle; $\zeta^{\mathrm{V}}=c_c/2m^{\mathrm{V}}\omega^{\mathrm{V}}$ is the damping ratio of the vehicle; $R(x)=r_c(\tilde{x})/L^{\mathrm{B}}$ is the scaled road roughness profile. Throughout this study *dot* denotes differentiation with respect to the dimensionless time τ (e.g., $\dot{u}^{\mathrm{V}}$), and *prime* (e.g., $R(x)'$) stands for differentiation with respect to the dimensionless position x. Equation (6) is a dimensionless version of Eq. (5) which offers advantages later to eliminate the negative effect of RRCs and to simplify the output signal for the ST-SSI method with fewer parameters that require measuring.

Accordingly, the EOM of the dimensionless response $\mathbf{u}^{\mathrm{B}}$ of the bridge (Eq. 4) becomes

$$\left(\omega^{\mathrm{V}}\right)^2\mathbf{M}^{\mathrm{B}}\ddot{\mathbf{u}}^{\mathrm{B}}+\omega^{\mathrm{V}}\mathbf{C}^{\mathrm{B}}\dot{\mathbf{u}}^{\mathrm{B}}+\mathbf{K}^{\mathrm{B}}\mathbf{u}^{\mathrm{B}}=-\frac{1}{L^{\mathrm{B}}}\mathbf{W}_N^{\mathrm{B}}(x)\left(\tilde{\lambda}_N(\tau)+m^{\mathrm{V}}g\right). \quad (7)$$

Note that ω^{V} appears in dimensionless EOM of the bridge because of the differentiation with respect to the dimensionless time τ.

2.3 Elimination of the negative effect from road roughness profile

The next task is to address the negative effect from road roughness conditions (RRCs). To eliminate the effect due to RRCs, the present study builds on the premise of the Yang et al. (2012) and Kim et al. (2016) approach. Specifically, instead of using two connected vehicles/wheels (Yang et al., 2012; Kim et al., 2016), this study proposes two runs over the bridge with the same test-vehicle but at different speeds. The key is that during the two runs the test-vehicle traverses the same road roughness profile, which allows its elimination as follows.

Consider a test-vehicle (with frequency ω^{V}) crossing the same bridge twice: the first time with speed v_1 and the second with speed v_2. The irregularity profile $r_c(\check{x})$ at any position $\check{x}$ on the bridge deck remains the same during all runs. Accordingly, at the (dimensionless) position $x = \check{x}/L^{\mathrm{B}}$ the (dimensionless) roughness profile would be the same $R(x)$. The subtraction of the (left-hand sides) LHS of Equation (6) thus returns

$$\Delta P = \left({}_{(1)}\lambda_N(t) - {}_{(2)}\lambda_N(t)\right) + \left({}_{(1)}u^{\mathrm{V}} - {}_{(2)}u^{\mathrm{V}}\right) + 2\zeta^{\mathrm{V}}\left({}_{(1)}\dot{u}^{\mathrm{V}} - {}_{(2)}\dot{u}^{\mathrm{V}}\right) = \Delta\lambda_N(t) + \Delta u^{\mathrm{V}} + 2\zeta^{\mathrm{V}}\Delta\dot{u}^{\mathrm{V}} \tag{8}$$

where the left-subscript ${}_{(i)}(\,)$ denotes the parameter for i-th run. Accordingly, the subtraction of the (right-hand sides) RHS of Equation (6) gives

$$\begin{aligned}\Delta P = &\left(\mathbf{W}_N^{\mathrm{B}}(x)^{\mathrm{T}} + \frac{2v_1\zeta^{\mathrm{V}}}{\omega^{\mathrm{V}}L^{\mathrm{B}}}\mathbf{W}_N^{\mathrm{B}}(x)'^{\mathrm{T}}\right)\left({}_{(1)}\mathbf{u}^{\mathrm{B}} - {}_{(2)}\mathbf{u}^{\mathrm{B}}\right) + 2\zeta^{\mathrm{V}}\mathbf{W}_N^{\mathrm{B}}(x)^{\mathrm{T}}\left({}_{(1)}\dot{\mathbf{u}}^{\mathrm{B}} - {}_{(2)}\dot{\mathbf{u}}^{\mathrm{B}}\right) \\ &+\alpha R(x)' + \alpha\mathbf{W}_N^{\mathrm{B}}(x)'^{\mathrm{T}}\,{}_{(2)}\mathbf{u}^{\mathrm{B}}\end{aligned} \tag{9}$$

where α is a coefficient that depends on the difference between the two speeds

$$\alpha = \frac{2\zeta^{\mathrm{V}}}{\omega^{\mathrm{V}}L^{\mathrm{B}}}(v_1 - v_2). \tag{10}$$

Notice that Eq.(9) does not depend on the RRC profile $R(x)$, but solely on the slope of the irregularities $R(x)'$. Equation (9) would be directly applicable to the proposed ST-SSI formulation (Eq. 2) if the $\alpha\left(R(x)' + \mathbf{W}_N^{\mathrm{B}}(x)'^{\mathrm{T}}\,{}_{(2)}\mathbf{u}^{\mathrm{B}}\right)$ term was a zero-mean white noise. The spatial derivative of RRC $R(x)'$ is generally white noise (ISO 8608, 2016), however, $\mathbf{W}_N^{\mathrm{B}}(x)'^{\mathrm{T}}\,{}_{(2)}\mathbf{u}^{\mathrm{B}}$ cannot be assumed to be white noise. Nevertheless, choosing the speed of each run, and hence the value of the coefficient α (Eq. 10), allows to eliminate the $\alpha\mathbf{W}_N^{\mathrm{B}}(x)'^{\mathrm{T}}\,{}_{(2)}\mathbf{u}^{\mathrm{B}}$ term from the output signal ΔP.

To elucidate, consider the order of magnitude $O(\,)$ of the terms involved in the output signal ΔP (Eq. 8) and the RHS (Eq. 9) of the subtracted EOMs of the vehicle. In particular, the dimensionless displacement response of the vehicle and the bridge are approximately of $O\left({}_{(i)}u^{\mathrm{V}}\right) \approx 10^{-3}$ and $O\left({}_{(i)}u^{\mathrm{B}}\right) \approx 10^{-3}$. Accordingly, the orders of magnitude of the dimensionless velocity and acceleration response of the vehicle are

$$O\left({}_{(i)}\dot{u}^{\mathrm{V}}\right) = O\left(\frac{1}{\omega^{\mathrm{V}}L^{\mathrm{B}}}\frac{d}{dt}\,{}_{(i)}\tilde{u}^{\mathrm{V}}\right) = O\left(\frac{1}{\omega^{\mathrm{V}}L^{\mathrm{B}}}\frac{{}_{(i)}\tilde{u}^{\mathrm{V}}}{T^{\mathrm{V}}}\right) = O\left(\frac{1}{2\pi}\,{}_{(i)}u^{\mathrm{V}}\right) \approx 10^{-4} \tag{11}$$

186 $$O\left({}_{(i)}\ddot{u}^{\mathrm{V}}\right)=O\left(\frac{1}{\left(\omega^{\mathrm{V}}\right)^2 L^{\mathrm{B}}}\frac{d^2}{dt^2}{}_{(i)}\tilde{u}^{\mathrm{V}}\right)=O\left(\frac{1}{\left(\omega^{\mathrm{V}}\right)^2 L^{\mathrm{B}}}\frac{{}_{(i)}\tilde{u}^{\mathrm{V}}}{\left(T^{\mathrm{V}}\right)^2}\right)=O\left(\frac{1}{4\pi^2}{}_{(i)}u^{\mathrm{V}}\right)\approx 10^{-4} \quad (12)$$

187 Dividing Eq. (3) by $m^{\mathrm{V}}\left(\omega^{\mathrm{V}}\right)^2 L^{\mathrm{B}}$ gives the order of the dimensionless contact force as
188 $O\left({}_{(i)}\lambda_N(t)\right)=O\left({}_{(i)}\ddot{u}^{\mathrm{V}}\right)=10^{-4}$. The damping ratio of the vehicle ζ^{V} is of the order $O\left(\zeta^{\mathrm{V}}\right)=10^{-1}$,
189 with practical values between 0.3 and 0.6. Consequently, it follows that the order of magnitude of
190 the output signal (Eq. 8) is $O(\Delta P)\approx 10^{-3}$.

191 Focusing on the $\mathbf{W}_N^{\mathrm{B}}(x)'^{\mathrm{T}}{}_{(2)}\mathbf{u}^{\mathrm{B}}$ term, the matrix $\mathbf{W}_N^{\mathrm{B}}(x)$ is composed of shape functions and
192 therefore $O\left(\mathbf{W}_N^{\mathrm{B}}(x)\right)=1$ and $O\left(\mathbf{W}_N^{\mathrm{B}}(x)'\right)\approx 10^2$ (see Appendix A.1). Consequently, the order of
193 magnitude of $\mathbf{W}_N^{\mathrm{B}}(x)'^{\mathrm{T}}{}_{(2)}\mathbf{u}^{\mathrm{B}}$ is approximately $O\left(\mathbf{W}_N^{\mathrm{B}}(x)'^{\mathrm{T}}{}_{(2)}\mathbf{u}^{\mathrm{B}}\right)\approx 10^0$. Hence, an appropriate
194 selection of the two speeds, v_1 and v_2, limits the value of the coefficient α

195 $$\alpha=\frac{2\zeta^{\mathrm{V}}}{\omega^{\mathrm{V}}L^{\mathrm{B}}}(v_1-v_2)\le 10^{-3} \quad (13)$$

196 and allows to neglect the term $\alpha\mathbf{W}_N^{\mathrm{B}}(x)'^{\mathrm{T}}{}_{(2)}\mathbf{u}^{\mathrm{B}}$ from the output signal ΔP, as
197 $O\left(\alpha\mathbf{W}_N^{\mathrm{B}}(x)'^{\mathrm{T}}{}_{(2)}\mathbf{u}^{\mathrm{B}}\right)\le 10^{-4}$.

198 Then, Eq. (9) becomes approximately

199 $$\Delta P\simeq\left(\mathbf{W}_N^{\mathrm{B}}(x)^{\mathrm{T}}+\frac{2v_1\zeta^{\mathrm{V}}}{\omega^{\mathrm{V}}L^{\mathrm{B}}}\mathbf{W}_N^{\mathrm{B}}(x)'^{\mathrm{T}}\right)\left({}_{(1)}\mathbf{u}^{\mathrm{B}}-{}_{(2)}\mathbf{u}^{\mathrm{B}}\right)+2\zeta^{\mathrm{V}}\mathbf{W}_N^{\mathrm{B}}(x)^{\mathrm{T}}\left({}_{(1)}\dot{\mathbf{u}}^{\mathrm{B}}-{}_{(2)}\dot{\mathbf{u}}^{\mathrm{B}}\right). \quad (14)$$

200 Equations (8) and (14) establish the relationship between the vehicle and bridge response.

201

202 **2.4 Problem formulation for an MDOF vehicle model**

203 This section formulates the proposed ST-SSI method for a multi-degree-of-freedom (MDOF) vehicle
204 model (Fig. 2a). Specifically, consider a vehicle with $r=2$ wheels (Fig. 2a) and a simply supported
205 beam (same as Fig. 1). The EOM of the vehicle is (Zeng et al., 2016; Stoura & Dimitrakopoulos, 2020;
206 Stoura & Dimitrakopoulos, accepted)

207 $$\mathbf{M}^{\mathrm{V}}\frac{d^2}{dt^2}\tilde{\mathbf{u}}^{\mathrm{V}}(t)+\mathbf{K}^{\mathrm{V}}\tilde{\mathbf{u}}^{\mathrm{V}}(t)+\mathbf{C}^{\mathrm{V}}\frac{d}{dt}\tilde{\mathbf{u}}^{\mathrm{V}}(t)-\mathbf{W}_N^{\mathrm{V}}\tilde{\boldsymbol{\lambda}}_N(t)=\mathbf{0} \quad (15)$$

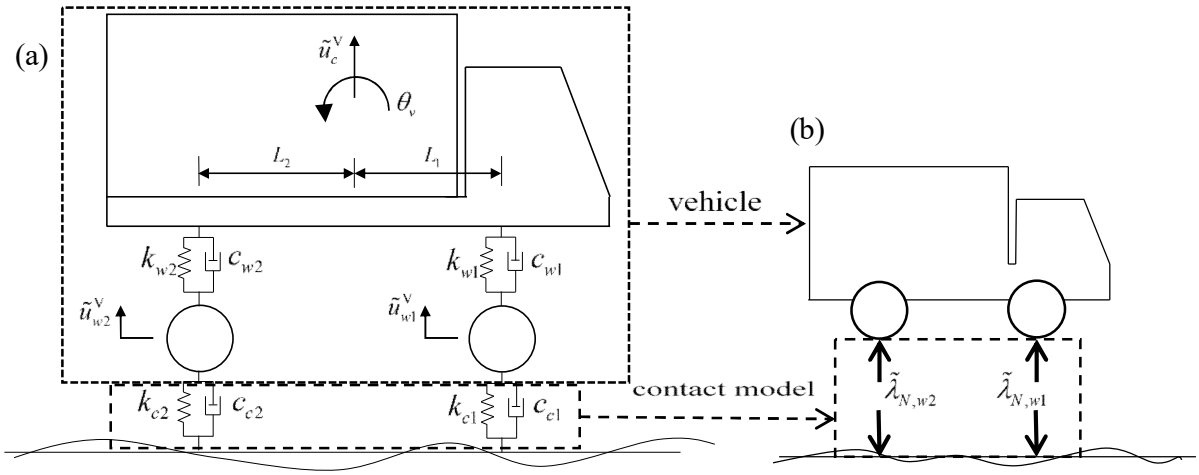

Figure 2. An MDOF vehicle model

where $\mathbf{M}^{\mathrm{V}}$, $\mathbf{K}^{\mathrm{V}}$ and $\mathbf{C}^{\mathrm{V}}$ are the mass, stiffness and damping matrices of the vehicle; $\tilde{\mathbf{u}}^{\mathrm{V}}(t)=\left[u_c^{\mathrm{V}} \quad \theta_v \quad u_{w1}^{\mathrm{V}} \quad u_{w2}^{\mathrm{V}}\right]^{\mathrm{T}}$ is the vehicle displacement vector; $\mathbf{W}_N^{\mathrm{V}}$ is the matrix denoting the DOFs for the wheels; and $\tilde{\boldsymbol{\lambda}}_N(t)=\left[\lambda_{N,w1} \quad \lambda_{N,w2}\right]^{\mathrm{T}}$ is the contact force vector as Eq. (5) with $k_c = k_{cj}$, $c_c = c_{cj}$, $\tilde{u}^{\mathrm{V}}(t)=u_{wj}^{\mathrm{V}}(t)$, $\mathbf{W}_N^{\mathrm{B}}(x)=\mathbf{W}_{Nj}^{\mathrm{B}}(x)$ and $r_c(x)=r_{cj}(x)$. Here j in the subscript denotes j-th wheel of the vehicle.

What matters for the application of the proposed ST-SSI method is the interaction relationship between vehicle and bridge. This allows to simplify the VBI model ignoring the details of the vehicle and focusing on the contact force $\tilde{\lambda}_{N,wj}$ connecting the vehicle and bridge (Fig. 2b). Similar to Eq. (6), using the dimensionless time $\tau=\omega_1^{\mathrm{V}}t$ gives the dimensionless contact force $\lambda_{N,wj}$ of j-th (j = 1,2,…,r) wheel as

$$\begin{aligned}&\lambda_{N,wj}+K_{cj}^{\mathrm{V}}u_{wj}^{\mathrm{V}}+2C_{cj}^{\mathrm{V}}\dot{u}_{wj}^{\mathrm{V}}\\&=\left(K_{cj}^{\mathrm{V}}\mathbf{W}_{Nj}^{\mathrm{B}}(x)^{\mathrm{T}}+\frac{2v_iC_{cj}^{\mathrm{V}}}{\omega_1^{\mathrm{V}}L^{\mathrm{B}}}\mathbf{W}_{Nj}^{\mathrm{B}}(x)'^{\mathrm{T}}\right)\mathbf{u}^{\mathrm{B}}+2C_{cj}^{\mathrm{V}}\mathbf{W}_{Nj}^{\mathrm{B}}(x)^{\mathrm{T}}\dot{\mathbf{u}}^{\mathrm{B}}+K_{cj}^{\mathrm{V}}R_j(x)+\frac{2v_iC_{cj}^{\mathrm{V}}}{\omega_1^{\mathrm{V}}L^{\mathrm{B}}}R_j(x)'\end{aligned}\tag{16}$$

where m_1^{V} and ω_1^{V} are the first modal mass and frequency of the vehicle, respectively; $\lambda_{N,wj}=\tilde{\lambda}_{N,wj}(\tau)/m_1^{\mathrm{V}}\left(\omega_1^{\mathrm{V}}\right)^2L^{\mathrm{B}}$ is the dimensionless contact force; $u_{wj}^{\mathrm{V}}=\tilde{u}_{wj}^{\mathrm{V}}(\tau)/L^{\mathrm{B}}$ denotes the dimensionless displacement response of j-th wheel of the vehicle; $K_{cj}^{\mathrm{V}}=k_{cj}/m_1^{\mathrm{V}}\left(\omega_1^{\mathrm{V}}\right)^2$ is the stiffness ratio and $C_{cj}^{\mathrm{V}}=c_{cj}/2m_1^{\mathrm{V}}\omega_1^{\mathrm{V}}$ is the damping ratio of j-th wheel of the vehicle.

Dividing Eq.(16) by K_{cj}^{V} and subtracting Eq.(16) for two runs, eliminates the road roughness profile $R_j(x)$ from equation (16). So the subtraction ΔP of the LHS of Eq.(16) for two runs gives

$$\Delta P = \frac{1}{K_{cj}^{\mathrm{V}}}\Delta\lambda_{N,wj} + \Delta u_{wj}^{\mathrm{V}} + \frac{2C_{cj}^{\mathrm{V}}}{K_{cj}^{\mathrm{V}}}\Delta\dot{u}_{wj}^{\mathrm{V}} \tag{17}$$

where $\Delta\lambda_{N,wj}$ is the difference of the dimensionless contact forces in the two runs; $\Delta u_{wj}^{\mathrm{V}}$ and $\Delta\dot{u}_{wj}^{\mathrm{V}}$ are the differences between the displacement and velocity response for the two runs, respectively

Accordingly the subtraction of the RHS of Eq.(16) for two runs is

$$\begin{aligned}\Delta P = &\left(\mathbf{W}_{Nj}^{\mathrm{B}}(x)^{\mathrm{T}} + \frac{2v_1 C_{cj}^{\mathrm{V}}}{\omega_1^{\mathrm{V}} L^{\mathrm{B}} K_{cj}^{\mathrm{V}}}\mathbf{W}_{Nj}^{\mathrm{B}}(x)'^{\mathrm{T}}\right)\left({}_{(1)}\mathbf{u}^{\mathrm{B}} - {}_{(2)}\mathbf{u}^{\mathrm{B}}\right) + \frac{2C_{cj}^{\mathrm{V}}}{K_{cj}^{\mathrm{V}}}\mathbf{W}_{Nj}^{\mathrm{B}}(\tilde{x})^{\mathrm{T}}\left({}_{(1)}\dot{\mathbf{u}}^{\mathrm{B}} - {}_{(2)}\dot{\mathbf{u}}^{\mathrm{B}}\right) \\ &+\alpha R_j(x)' + \alpha\,\mathbf{W}_{Nj}^{\mathrm{B}}(x)'^{\mathrm{T}}\,{}_{(2)}\mathbf{u}^{\mathrm{B}}\end{aligned} \tag{18}$$

where again α is a coefficient that depends on the difference of two speeds

$$\alpha = \frac{2C_{cj}^{\mathrm{V}}}{\omega_1^{\mathrm{V}} L^{\mathrm{B}} K_{cj}^{\mathrm{V}}}(v_1 - v_2) \le 10^{-3}. \tag{19}$$

Similar to the SDOF vehicle model, the $\alpha\,\mathbf{W}_{Nj}^{\mathrm{B}}(x)'^{\mathrm{T}}\,{}_{(2)}\mathbf{u}^{\mathrm{B}}$ term is ignorable compared to the output signal ΔP if α is sufficiently small (e.g., $\alpha \le 10^{-3}$). Finally, Eq. (18) becomes the same as Eq. (14) with $\mathbf{W}_N^{\mathrm{B}}(x) = \mathbf{W}_{Nj}^{\mathrm{B}}(x)$, $\omega^{\mathrm{V}} = \omega_1^{\mathrm{V}}$ and $\zeta^{\mathrm{V}} = C_{cj}^{\mathrm{V}}/K_{cj}^{\mathrm{V}}$.

2.5 Formulation of VBI problem for system identification

To cast the equations of the VBI problem (Eqs. 7 and 14) into a suitable form for the needs of the proposed ST-SSI method, Eq.(14) must take the form of Eq.(2). To this end, we re-write Eq.(14) in state space as

$$\Delta P = \mathbf{N}^{\mathrm{V}f}\mathbf{N}^{\mathrm{WB}}(x)\Delta\mathbf{X}^{\mathrm{B}}(\tau) \tag{20}$$

where $\Delta\mathbf{X}^{\mathrm{B}}(\tau)$ is the state vector

$$\Delta\mathbf{X}^{\mathrm{B}}(\tau) = {}_{(1)}\mathbf{X}^{\mathrm{B}} - {}_{(2)}\mathbf{X}^{\mathrm{B}} = \begin{bmatrix} {}_{(1)}\mathbf{u}^{\mathrm{B}} \\ \omega^{\mathrm{V}}\,{}_{(1)}\dot{\mathbf{u}}^{\mathrm{B}} \end{bmatrix} - \begin{bmatrix} {}_{(2)}\mathbf{u}^{\mathrm{B}} \\ \omega^{\mathrm{V}}\,{}_{(2)}\dot{\mathbf{u}}^{\mathrm{B}} \end{bmatrix} = \begin{bmatrix} {}_{(1)}\mathbf{u}^{\mathrm{B}} - {}_{(2)}\mathbf{u}^{\mathrm{B}} \\ \omega^{\mathrm{V}}\left({}_{(1)}\dot{\mathbf{u}}^{\mathrm{B}} - {}_{(2)}\dot{\mathbf{u}}^{\mathrm{B}}\right) \end{bmatrix} \in R^{2N\times 1}, \tag{21}$$

$\mathbf{N}^{Vf}$ and $\mathbf{N}^{\mathrm{WB}}(x)$ are system matrices defined as

$$\mathbf{N}^{Vf} = \begin{bmatrix} 1 & \frac{2\zeta^{\mathrm{V}}}{\omega^{\mathrm{V}}} \end{bmatrix} \tag{22}$$

and

$$\mathbf{N}^{\mathrm{WB}}(x) = \begin{bmatrix} \mathbf{W}_N^{\mathrm{B}}(x)^{\mathrm{T}} & \mathbf{0} \\ \frac{v_1}{L^{\mathrm{B}}}\mathbf{W}_N^{\mathrm{B}}(x)'^{\mathrm{T}} & \mathbf{W}_N^{\mathrm{B}}(x)^{\mathrm{T}} \end{bmatrix} \in R^{2\times 2N} \tag{23}$$

respectively. The equation of output signal (Eq. 20) in state space takes now the time-discrete form

$$\Delta P_k = \mathbf{N}^{Vf}\mathbf{N}_k^{\mathrm{WB}}\Delta\mathbf{X}_k^{\mathrm{B}} \tag{24}$$

where ΔP_k is the known output signal related to the vehicle, $\Delta\mathbf{X}_k^{\mathrm{B}}$ is the state vector at time step k, and $\mathbf{N}_k^{\mathrm{WB}}$ is the matrix related to the position of the vehicle in time-discrete form.

To cast the EOM of the bridge subsystem (Eq. 7) into the form of Eq.(1), we write the EOM of the bridge (Eq. 7) for i-th run in state space

$${}_{(i)}\dot{\mathbf{X}}^{B} = \mathbf{N}_c^{\mathrm{B}}{}_{(i)}\mathbf{X}^{B} + \frac{1}{L^{\mathrm{B}}}\mathbf{N}_c^{M}\mathbf{W}_N^{\mathrm{B}}(x)\left({}_{(i)}\tilde{\lambda}_N(\tau) + m^{\mathrm{V}}g\right) \tag{25}$$

where $\mathbf{N}_c^{\mathrm{B}}$ is the time-invariant bridge system matrix

$$\mathbf{N}_c^{\mathrm{B}} = \begin{bmatrix} \mathbf{0} & \mathbf{I} \\ -\left(\mathbf{M}^{\mathrm{B}}\right)^{-1}\mathbf{K}^{\mathrm{B}} & -\left(\mathbf{M}^{\mathrm{B}}\right)^{-1}\mathbf{C}^{\mathrm{B}} \end{bmatrix} \in R^{2N\times 2N}, \tag{26}$$

and $\mathbf{N}_c^{M}$ is a matrix which includes the mass of the bridge

$$\mathbf{N}_c^{M} = \begin{bmatrix} \mathbf{0} \\ -\left(\mathbf{M}^{\mathrm{B}}\right)^{-1} \end{bmatrix} \in R^{2N\times N}. \tag{27}$$

Then we convert the state space EOM of the bridge (Eq. 25) to a time-discrete form, by multiplying each side of Eq.(25) with $\exp\left(-\mathbf{N}_c^{\mathrm{B}}t\right)$. After integration (Yang & Chen, 2015), the transformed equation is

$${}_{(i)}\mathbf{X}_{k+1}^{\mathrm{B}} = \mathbf{N}^{\mathrm{B}}{}_{(i)}\mathbf{X}_k^{\mathrm{B}} + \frac{1}{L^{\mathrm{B}}}\mathbf{N}^{M}\mathbf{W}_{N,k}^{\mathrm{B}}\left({}_{(i)}\tilde{\lambda}_{N,k} + m^{\mathrm{V}}g\right) \tag{28}$$

where k in the subscript indicates the time step, $\mathbf{N}^{\mathrm{B}}$ is the system matrix of the bridge in time-discrete form

$$\mathbf{N}^{\mathrm{B}} = \exp\left(-\mathbf{N}_c^{\mathrm{B}}\Delta t\right) \in R^{2N\times 2N}, \tag{29}$$

and $\mathbf{N}^{M}$ is the time-discrete matrix

$$\mathbf{N}^{M} = \left(\mathbf{N}_c^{\mathrm{B}}\right)^{-1}\left(\mathbf{N}^{\mathrm{B}} - \mathbf{I}\right)\mathbf{N}_c^{M} \in R^{2N\times N}. \tag{30}$$

Lastly, the subtraction of EOMs of the bridge in time-discrete form (Eq. 28) for two runs yields

$$\Delta\mathbf{X}_{k+1}^{\mathrm{B}} = \mathbf{N}^{\mathrm{B}}\Delta\mathbf{X}_k^{\mathrm{B}} + \frac{1}{L^{\mathrm{B}}}\mathbf{N}^{M}\mathbf{W}_{N,k}^{\mathrm{B}}\Delta\lambda_{N,k} \tag{31}$$

where $\Delta\lambda_{N,k}$ is the difference between the contact forces in two runs at time step k. Note that the gravity term $m^{\mathrm{V}}g$ disappears after the subtraction. Collectively, Eqs.(31) and (24) are suitable for the application of the proposed ST-SSI method.

2.6 Application of ST-SSI to the time-varying VBI system

Short-time stochastic subspace identification (ST-SSI) allows for time-varying system matrices provided that this time-variation is much slower than the dynamics of the system during the examined time-interval (Ohsumi & Kawano, 2002; Marchesiello et al., 2009). In the context of the VBI problem, this implies that both system matrices i.e., $\mathbf{N}^{\mathrm{B}}$ in Eq. (31) and $\mathbf{N}^{\mathrm{V}f}\mathbf{N}_k^{\mathrm{WB}}$ in Eq. (24) should approximately be time-invariant. Matrices $\mathbf{N}^{\mathrm{B}}$ and $\mathbf{N}^{\mathrm{V}f}$ are time-invariant. The system matrix $\mathbf{N}_k^{\mathrm{WB}}$ (Eq.23 with $x=vk\Delta t$) in Eq. (24) though depends on the location of the vehicle (contact force) and hence it varies with time. This time variation depends on the speed of the vehicle and is characterized by loading frequency ω_{Ln} (Yang et al., 2004b):

$$\omega_{Ln} = \frac{n\pi v}{L_{eff}} \tag{32}$$

where L_{eff} is the characteristic length of a bridge. For a simply supported beam, the characteristic length L_{eff} is equal to the length of the bridge L^{B}. The dimensionless speed parameter $S_{vn} = \omega_{Ln}/\omega_n^{\mathrm{B}}$ scales the loading frequency ω_{Ln} with the bridge frequency ω_n^{B} (Yang et al., 2004b). Usually, the

first mode (n=1) of the bridge is the most dominant during vehicle-bridge interaction, especially for simply supported bridges (Stoura & Dimitrakopoulos, 2020; Stoura & Dimitrakopoulos, accepted). If the dimensionless driving speed S_{v1} is small (e.g., $S_{v1}<0.1$), the excitation from the moving contact force is much slower compared with the structural dynamics of the bridge. Consequently, the time-variation (of system matrix $\mathbf{N}_k^{\mathrm{WB}}$) is ignorable for the needs of bridge identification using ST-SSI. For a generic bridge with fundamental frequency around 5Hz and length L^{B} between 15m and 50m, the $S_{v1}<0.1$ assumption defines an upper limit for the speed to be between 54km/h for L^{B}=15m until 180km/h for L^{B}=50m. Therefore, for most cases of practical interest the assumption $S_{v1}<0.1$ can be satisfied, which implies also that the proposed ST-SSI approach is applicable.

Combining the two equations Eqs. (31) and (24) gives the data equation of the output signal

$$\Delta P_k=\mathbf{N}^{\mathrm{V}f}\mathbf{N}_k^{\mathrm{WB}}\left(\mathbf{N}^{\mathrm{B}}\right)^{k-1}\Delta\mathbf{X}_1^{\mathrm{B}}+\mathbf{N}^{\mathrm{V}f}\mathbf{N}_k^{\mathrm{WB}}\sum\nolimits_{q=1}^{k-1}\left(\mathbf{N}^{\mathrm{B}}\right)^{k-q-1}\mathbf{N}^{M}\mathbf{W}_{N,q}^{\mathrm{B}}\Delta\dot{\lambda}_{N,q} \tag{33}$$

where $\Delta\mathbf{X}_1^{\mathrm{B}}$ stands for the initial state of vector $\Delta\mathbf{X}_k^{\mathrm{B}}$. To apply the ST-SSI method, we need to construct the Hankel matrix using the measured output signal ΔP_k. Then, the Hankel matrix is divided into the "past" part denoted with superscript $(\ )^p$ and the "future" part with superscript $(\ )^f$

$$\mathbf{H}_{\mathbf{p}}=\begin{bmatrix}\mathbf{H}_{\mathbf{p}}^{p}\\ \mathbf{H}_{\mathbf{p}}^{f}\end{bmatrix}=\begin{bmatrix}\Delta P_1 & \cdots & \Delta P_{col}\\ \vdots & \ddots & \vdots\\ \Delta P_s & \cdots & \Delta P_{s+col-1}\\ \Delta P_{s+1} & \cdots & \Delta P_{s+col}\\ \vdots & \ddots & \vdots\\ \Delta P_{2s} & \cdots & \Delta P_{2s+col-1}\end{bmatrix}\in R^{2s\times col} \tag{34}$$

where $2s$ is the number of rows in the Hankel matrix which is usually at least tenfold of the DOFs of the bridge system; col is the number of columns in the Hankel matrix; and $(2s+col-1)$ is the total number of data entries.

Substituting the data equation (Eq. 33) into the Hankel matrix (Eq. 34) yields

$$\mathbf{H}_{\mathbf{p}}=\begin{bmatrix}\mathbf{H}_{\mathbf{p}}^{p}\\ \mathbf{H}_{\mathbf{p}}^{f}\end{bmatrix}=\begin{bmatrix}\mathbf{\Gamma}\mathbf{X}^{p}+\mathbf{\Psi}\mathbf{D}_N\mathbf{U}^{p}\\ \mathbf{\Gamma}\mathbf{X}^{f}+\mathbf{\Psi}\mathbf{D}_N\mathbf{U}^{f}\end{bmatrix} \tag{35}$$

where $\mathbf{\Gamma}$ is the observability matrix containing the unknown bridge system matrix $\mathbf{N}^{\mathrm{B}}$, expressed as

$$\mathbf{\Gamma}=\left[\left(\mathbf{N}^{\mathrm{V}f}\mathbf{N}_k^{\mathrm{WB}}\right)^{\mathrm{T}}\quad\left(\mathbf{N}^{\mathrm{V}f}\mathbf{N}_k^{\mathrm{WB}}\mathbf{N}^{\mathrm{B}}\right)^{\mathrm{T}}\quad\cdots\quad\left(\mathbf{N}^{\mathrm{V}f}\mathbf{N}_k^{\mathrm{WB}}\left(\mathbf{N}^{\mathrm{B}}\right)^{s-1}\right)^{\mathrm{T}}\right]^{\mathrm{T}}\in R^{s\times 2N_0}. \tag{36}$$

where N_o is the estimated system order in the identification process, which is similar to the DOFs of the bridge. The proposed ST-SSI method usually begins with a small system order (e.g., $N_o=2$), and repeats the identification procedure with increasing system orders until the identification results become stable. In general, this cycle may not terminate until the estimated system order N_o is larger than the DOFs required for the corresponding bridge modes. Appendix 5.2 gives details of the remaining matrices of Eq.(35).

Both Hankle matrices ("past" $\mathbf{H}_{\mathbf{p}}^{p}$ and "future" $\mathbf{H}_{\mathbf{p}}^{f}$) in Eq.(35) have two components: (i) $\mathbf{\Gamma X}^{p}$ and $\mathbf{\Gamma X}^{f}$ related to the bridge, and (ii) $\mathbf{\Psi D}_N\mathbf{U}^{p}$ and $\mathbf{\Psi D}_N\mathbf{U}^{f}$ related to the position and magnitude of the contact force. For the needs of ST-SSI, the next step is to remove the components unrelated to the bridge (i.e., $\mathbf{\Psi D}_N\mathbf{U}^{p}$ and $\mathbf{\Psi D}_N\mathbf{U}^{f}$) from the known Hankel matrices (i.e., $\mathbf{H}_{\mathbf{p}}^{p}$ and $\mathbf{H}_{\mathbf{p}}^{f}$). Projecting the "future" Hankel matrix $\mathbf{H}_{\mathbf{p}}^{f}$ onto the "past" Hankel matrix $\mathbf{H}_{\mathbf{p}}^{p}$ (Van Overschee & De Moor, 2012) gives

$$\mathrm{proj}_{\mathbf{H}_{\mathbf{p}}^{p}}\left(\mathbf{H}_{\mathbf{p}}^{f}\right)=\mathrm{proj}_{\mathbf{X}^{p}}\left(\mathbf{\Gamma X}^{f}\right)+\mathrm{proj}_{\mathbf{X}^{p}}\left(\mathbf{\Psi D}_N\mathbf{U}^{f}\right)+\mathrm{proj}_{\mathbf{U}^{p}}\left(\mathbf{\Gamma X}^{f}\right)+\mathrm{proj}_{\mathbf{U}^{p}}\left(\mathbf{\Psi D}_N\mathbf{U}^{f}\right). \tag{37}$$

It is evident that the "future" contact force $\mathbf{\Psi D}_N\mathbf{U}^{f}$ does not affect the "past" bridge response $\mathbf{\Gamma X}^{p}$, hence $\mathrm{proj}_{\mathbf{X}^{p}}\left(\mathbf{\Psi D}_N\mathbf{U}^{f}\right)=0$. Further, for the assumed dimensionless speed S_{v1} values (i.e., $S_{v1}<0.1$) the dynamic magnification factor is close to 1. Thus, the dynamic response is minor compared with the static response (Yang et al., 2004b) and the "past" and "future" VBI systems become two independent problems. Then, the "past" and "future" contact forces (i.e., $\mathbf{\Psi D}_N\mathbf{U}^{p}$ and $\mathbf{\Psi D}_N\mathbf{U}^{f}$) become independent, which implies $\mathrm{proj}_{\mathbf{U}^{p}}\left(\mathbf{\Psi D}_N\mathbf{U}^{f}\right)=0$. Also, the "past" contact force $\mathbf{\Psi D}_N\mathbf{U}^{p}$ is unrelated to the "future" bridge response $\mathbf{\Gamma X}^{f}$, which means $\mathrm{proj}_{\mathbf{U}^{p}}\left(\mathbf{\Gamma X}^{f}\right)=0$. Consequently, the common part of the "past" $\mathbf{H}_{\mathbf{p}}^{p}$ and "future" $\mathbf{H}_{\mathbf{p}}^{f}$ only relates to the bridge, coming from $\mathbf{\Gamma X}^{p}$ and $\mathbf{\Gamma X}^{f}$ as

$$\mathrm{proj}_{\mathbf{H}_{\mathbf{p}}^{p}}\left(\mathbf{H}_{\mathbf{p}}^{f}\right)=\mathrm{proj}_{\mathbf{X}^{p}}\left(\mathbf{\Gamma X}^{f}\right)=\mathbf{\Gamma X}^{f}\mathbf{\Pi}_{\mathbf{X}^{p}} \tag{38}$$

where $\mathbf{\Pi}_{\mathbf{X}^p}$ denotes the subspace of the matrix $\mathbf{X}^p$. The outcome of the projection, matrix $\mathbf{\Gamma X}^f \mathbf{\Pi}_{\mathbf{X}^p}$, is equal to the matrix $\mathbf{L}_{21}\mathbf{Q}_1^{\mathrm{T}}$ from the LQ decomposition of the Hankel matrix (Appendix A.3)

$$\mathbf{H}_{\mathbf{p}} = \begin{bmatrix} \mathbf{H}_{\mathbf{p}}^{p} \\ \mathbf{H}_{\mathbf{p}}^{f} \end{bmatrix} = \begin{bmatrix} \mathbf{L}_{11} & \mathbf{0} \\ \mathbf{L}_{21} & \mathbf{L}_{22} \end{bmatrix} \begin{bmatrix} \mathbf{Q}_1^{\mathrm{T}} \\ \mathbf{Q}_2^{\mathrm{T}} \end{bmatrix} \in R^{2s \times col} \tag{39}$$

where the submatrices $\mathbf{L}_{11}, \mathbf{L}_{21}, \mathbf{L}_{22} \in R^{s \times s}$ are those of the lower triangular matrices generated by LQ decomposition, and the submatrices $\mathbf{Q}_1^{\mathrm{T}}, \mathbf{Q}_2^{\mathrm{T}} \in R^{s \times col}$ are both orthogonal matrices.

Lastly, the combination of the LQ decomposition and the orthogonal projection returns (Appendix A.3)

$$\mathbf{L}_{21} = \mathbf{\Gamma X}^f \mathbf{\Pi}_{\mathbf{X}^p} \mathbf{Q}_1 . \tag{40}$$

After establishing the relation between the observability matrix $\mathbf{\Gamma}$ and the known matrix $\mathbf{L}_{21}$, the proposed ST-SSI method can identify bridge frequencies by seeking a similar matrix of $\mathbf{\Gamma}$ and extracting the information related to the bridge, following the standard approach of SSI (Katayama, 2006).

In summary, the proposed method requires the measurement of the dimensionless residual contact force $\Delta\lambda_N$ ($\Delta\lambda_{N,wj}$), the dimensionless residual response Δu^{V} ($\Delta u_{wj}^{\mathrm{V}}$) and $\Delta \dot{u}^{\mathrm{V}}$ ($\Delta \dot{u}_{wj}^{\mathrm{V}}$), the damping ratio ζ^{V} (C_{cj}^{V}), and the vehicle frequency ω^{V} (ω_1^{V}) of the SDOF (MDOF) vehicle (respectively). In the case of an MDOF vehicle the method also requires the knowledge of the stiffness ratio K_{cj}^{V}, the contact stiffness k_{cj}, and the damping coefficient c_{cj}, of the wheel selected for measuring. Lastly, recall that the internal parameters of the vehicle are not required for the bridge system identification through ST-SSI, nor any parameter/measurement of the bridge.

3 Verification of ST-SSI with numerical simulations

This section validates the ST-SSI method numerically. To this end, it first simulates VBI by solving Eq.(3) (or Eq. 15 for the MDOF vehicle model accordingly) and Eq. (4) to compute the response of the vehicle. It then applies the ST-SSI method to the output signal ΔP (Eq. 8 for the SDOF vehicle and

Table 1. Properties of the bridge

Length L^B (m)	flexural rigidity EI (kNm^2)	per-unit-mass μ (kg/m)	f_1^B (Hz)	f_2^B (Hz)
30	2.05×10^8	3.6×10^4	4.15	16.19

Table 2. Properties of the test-vehicles

vehicle No.	m^V (kg)	k_c (N/m)	c_c (Ns/m)	ζ^V	f^V (Hz)
1	5000	2.84×10^5	3.77×10^4	0.5	1.2
2	5000	1.78×10^6	5.65×10^4	0.3	3
3	10000	9.87×10^6	2.51×10^5	0.4	5

Eq. 17 for the MDOF vehicle respectively) from the vehicle to identify bridge frequencies. Table 1 shows the properties of the target bridge (Yang & Yau, 2017) to be identified.

3.1 Numerical cases with SDOF vehicle model

Key to the success of the proposed ST-SSI method is to minimize the noise in the output signal ΔP by controlling the coefficient α so that $\alpha \le 10^{-3}$. Equation (13) implies that a vehicle with high frequency, small damping ratio, and similar driving speeds in two runs is preferred by the ST-SSI method. This section validates the ST-SSI method using three test-vehicles with different properties (Table 2) and considering the road roughness RRC=0(smooth), 1(very good), 2 (good), 3(average), and 4 (poor) (ISO 8608, 2016). As a proof of concept, the road roughness profiles for different levels considered in this study only differ in magnitude, but contain the same components in frequency-domain. For vehicle 1, the speeds for two runs are: v_1=9.8m/s (35.3km/h) and v_2=10m/s (36km/h) to satisfy the requirement of $\alpha \le 10^{-3}$. The corresponding dimensionless driving speeds are: ${}_{(1)}S_{v1}$=0.039 and ${}_{(2)}S_{v1}$=0.04, which are both smaller than 0.1; and loading frequencies are: ${}_{(1)}f_{L1}$=0.327Hz and ${}_{(2)}f_{L1}$=0.33Hz. For vehicle 2 and 3, the speeds for two runs are: v_1=9m/s (32.4km/h) and v_2=10m/s (36km/h); the corresponding dimensionless driving speeds are: ${}_{(1)}S_{v1}$=0.036 and ${}_{(2)}S_{v1}$=0.04; and loading frequencies are: ${}_{(1)}f_{L1}$=0.3Hz and ${}_{(2)}f_{L1}$=0.33Hz.

Figure 3 shows the stabilization diagrams (Katayama, 2006) for the identification results. The dash lines in Fig. 3 (and Fig.4-5 later on) indicate theoretical bridge frequencies, and the circles represent bridge frequencies identified by the proposed ST-SSI method. This study only considers the identification successful if the circles create a line without much variation as the estimated system order N_o increases. A quantitative criterion that quantifies the stability of identified frequencies (Van Overschee & De Moor, 2012) is

$$\left|\frac{f_{N_o} - f_{N_o-1}}{f_{N_o}}\right| \le \varepsilon_f \tag{41}$$

Where f_{N_0} is the identified frequency when the system order is N_o, and $\varepsilon_f = 1\%$ is the stability criterion value. The filled circles in the figures represent stable (identified) frequencies according to the stability criterion. In some cases, identified frequencies appear in pairs due to Doppler effect (Yang et al., 2004a). The shifted frequencies $f^{\mathrm{B}}_{n,left}$ and $f^{\mathrm{B}}_{n,right}$ of the bridge relate to the loading frequency ω_{Ln}, as

$$f^{\mathrm{B}}_{n,left} = f^{\mathrm{B}}_n - \omega_{Ln}/2\pi \quad \text{and} \quad f^{\mathrm{B}}_{n,right} = f^{\mathrm{B}}_n + \omega_{Ln}/2\pi\,. \tag{42}$$

As explained in Section 2.5, a dimensionless speed $S_{v1} < 0.1$ implies the loading frequency $\omega_{Ln}/2\pi$ (Hz) is small compared to the frequency of the bridge f^{B}_n. According to Eq.(42), the mean value of the two frequencies $f^{\mathrm{B}}_{n,left}$ and $f^{\mathrm{B}}_{n,right}$ returns the target identified frequency.

Further, the error ε^{id}_n compares the identified frequency f^{id}_n with the (actual) bridge frequency f^{B}_n

$$\varepsilon^{id}_n = \frac{\left|f^{id}_n - f^{\mathrm{B}}_n\right|}{f^{\mathrm{B}}_n}\,. \tag{43}$$

The identification by the proposed ST-SSI method is considered successful if (i) the error ε^{id}_n is smaller than 10%; and (ii) all identified frequencies belong to the bridge.

Vehicles 2 and 3 successfully estimate bridge frequencies according to the proposed ST-SSI method for both smooth and (more importantly) irregular road surface (Figure 3). In the presence of RRCs, redundant circles do appear in the stabilization diagrams, but the lines representing the two identified

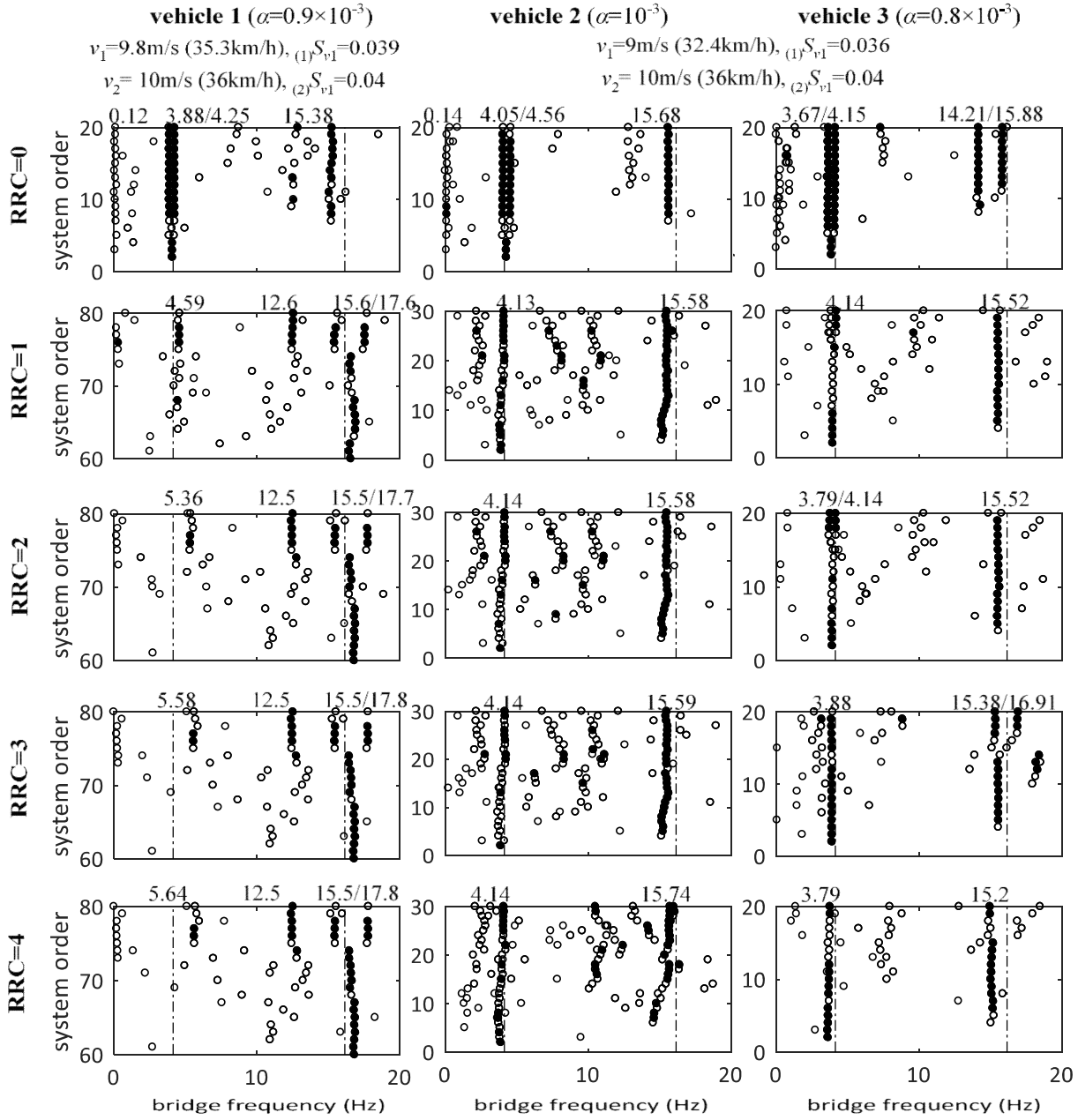

Figure 3. Stabilization diagrams for the identification results of ST-SSI (unit: Hz)

frequencies are clearly distinguishable and stable. Compared to vehicle 2, the heavier vehicle 3 excites more the bridge and leads to identification results with smaller noise. The small frequencies around 0.1Hz for the cases RRC=0 are attributed to numerical errors during the VBI analyses. Note that according to the stability criterion ε_f=1% (Eq. 41), this frequency is unstable and hence can be ignored. For the case of vehicle 1, ST-SSI identifies bridge frequencies successfully for the smooth road

Table 3. Identification results of the ST-SSI method

vehicle No.	RRC	f_1^{id} (Hz)	ε_1^{id}	f_2^{id} (Hz)	ε_2^{id}	redundant frequency
1	0	4.07	1.9%	15.38	5.0%	0.12Hz
	1	4.59	**10.6%**	16.60	1.2%	12.6Hz
	2	5.36	**29.2%**	16.60	1.2%	12.5Hz
	3	5.58	**34.5%**	16.65	2.8%	12.5Hz
	4	5.64	**35.9%**	16.65	2.8%	12.5Hz
2	0	4.31	3.9%	15.68	3.2%	0.14Hz
	1	4.13	2.9%	15.58	3.8%	-
	2	4.14	0.2%	15.58	3.8%	-
	3	4.14	0.2%	15.59	3.7%	-
	4	4.14	0.2%	15.74	2.8%	-
3	0	3.91	5.8%	15.05	7.0%	-
	1	4.14	0.2%	15.52	4.1%	-
	2	3.97	4.3%	15.52	4.1%	-
	3	3.88	6.5%	16.15	0.2%	-
	4	3.79	8.7%	15.20	6.1%	-

surface. However, the identifications considering RRCs are not good, especially for the fundamental frequency, even when limiting the coefficient α to $\alpha = 0.9\times10^{-3}$. The reason is that the speeds of vehicle 1 in the two runs are almost identical, which results in similar output signals from the two runs. Thus the subtraction of two output signals offers very little information about the bridge. Especially for the cases considering RRCs, the noise from the spatial derivative term $\alpha R(x)'$ in Eq.(9) could be too strong compared with the output signal ΔP, which worsens the identification. Thus, a special test-vehicle with deliberately high frequency, small damping ratio, and with a ratio of driving speeds not greater than 0.9, would be ideally configured to identify bridge frequencies according to the proposed ST-SSI method.

Table 3 summarizes the identified frequencies and corresponding errors. Vehicle 1 fails to identify the first frequency of the bridge especially in the presence of RRCs. It does identify in some cases the second frequency, but overall the results of the identification are characterized by redundant frequencies and errors. In contrast, vehicles 2 and 3 give good identification results for all cases examined, which is consistent with the conclusions obtained from Figure 3. Note that the identification results using vehicle 3 have larger but still acceptable errors compared with that from vehicle 2. Since the vehicle and bridge form a coupled VBI system, the moving vehicle may result in the frequency

variation of the bridge (Yang et al., 2013c). Such effect is ignorable if the vehicle mass is small compared with the bridge mass. However, if the vehicle is heavy the frequency variation should be taken into account, and a larger vehicle mass causes larger deviations in bridge frequencies. Hence it is essential to control also the mass of the test-vehicle.

3.2 Numerical cases with MDOF vehicle model

This section assesses the proposed ST-SSI method with a more realistic MDOF vehicle model (see Fig. 2). Table 4 summarizes the characteristics of the vehicle model, while further details can be found in Li et al. (2012). The present study applies the ST-SSI method assuming the rear-wheel of the vehicle monitors the response during the two runs, and considers the same road roughness conditions as Section 3.1 from RRC=0 (smooth) to 4 (poor) (ISO 8608, 2016).

Figure 4 shows the parameters (primarily combinations of speeds) for the two groups of numerical experiments (case 1 and case 2) examined and the pertinent identification results under different RRCs. As Figure 4 shows, it is feasible to control the coefficient α so that $\alpha \le 10^{-3}$ even for driving speeds as high as 20m/s (or 72km/h for case 2). As expected, the stabilization diagrams in Figure 4 (and Fig.5 later) are almost identical for different RRCs, since the proposed ST-SSI method has eliminated the effect due to RRCs from the output signal ΔP by limiting the coefficient α. Theoretically, smaller coefficient α should attribute to more similar identification results considering different RRCs. Overall, the proposed ST-SSI method is successful in identifying the fundamental frequency of the bridge even for high driving speed (20m/s or 72km/h for case 2) simultaneously with high levels of RRCs.

Table 4. Properties of MDOF vehicle model

m_1^{V} (kg)	$k_{c1}=k_{c2}$ (N/m)	$c_{c1}=c_{c2}$ (Ns/m)	f^{V} (Hz)	K_2^{V}	C_2^{V}
4990	7.02×10^5	1600	1.95	0.94	0.026

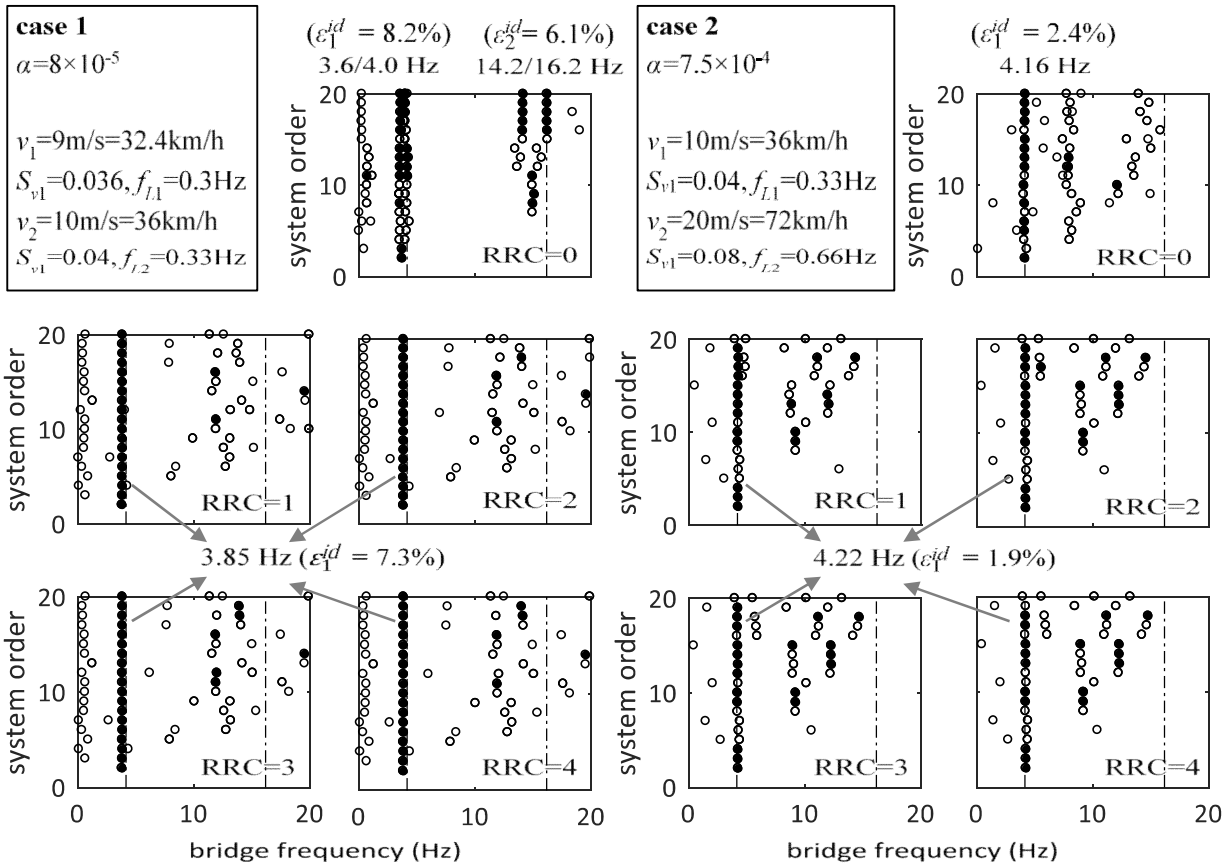

Figure 4. Stabilization diagrams for the identification results of ST-SSI with MDOF vehicle model

On the other hand, the proposed ST-SSI method fails to identify higher mode frequencies. One possible explanation is the inability of a single vehicle to excite higher modes of the bridge. Preliminary research from the authors (Jin et al., 2017; Jin et al., 2018) shows that on-going traffic could be beneficial to the identification of higher frequencies. To demonstrate this, Figure 5 considers a sequence of five vehicles with the properties of Table 4 and a spacing of d_v=30m between them, traversing the bridge of Table 1. The five vehicles traverse the bridge as a vehicle sequence twice with different driving speeds. Specifically, it applies the proposed ST-SSI method to the response of the rear-wheel of the last vehicle. In both cases of the vehicle sequence, ST-SSI successfully identifies the first two frequencies of the bridge. Comparing Figure 5 to Figure 4, the on-going traffic not only facilitates the identification of the second bridge frequency, but also reduces the noise in stabilization diagrams. In case 2, the high speed (20m/s or 72km/h) enhances the presence of vehicle frequency (2.05Hz) in the identification

when assuming the road surface is smooth. Nevertheless, this phenomenon only exists in the case of ideal road surface without any irregularities, which is unrealistic. In the presence of RRCs, even though the identification results of case 2 are not as stable as in case 1 in Figure 5, all the results are still acceptable (see Table 5 for the corresponding errors).

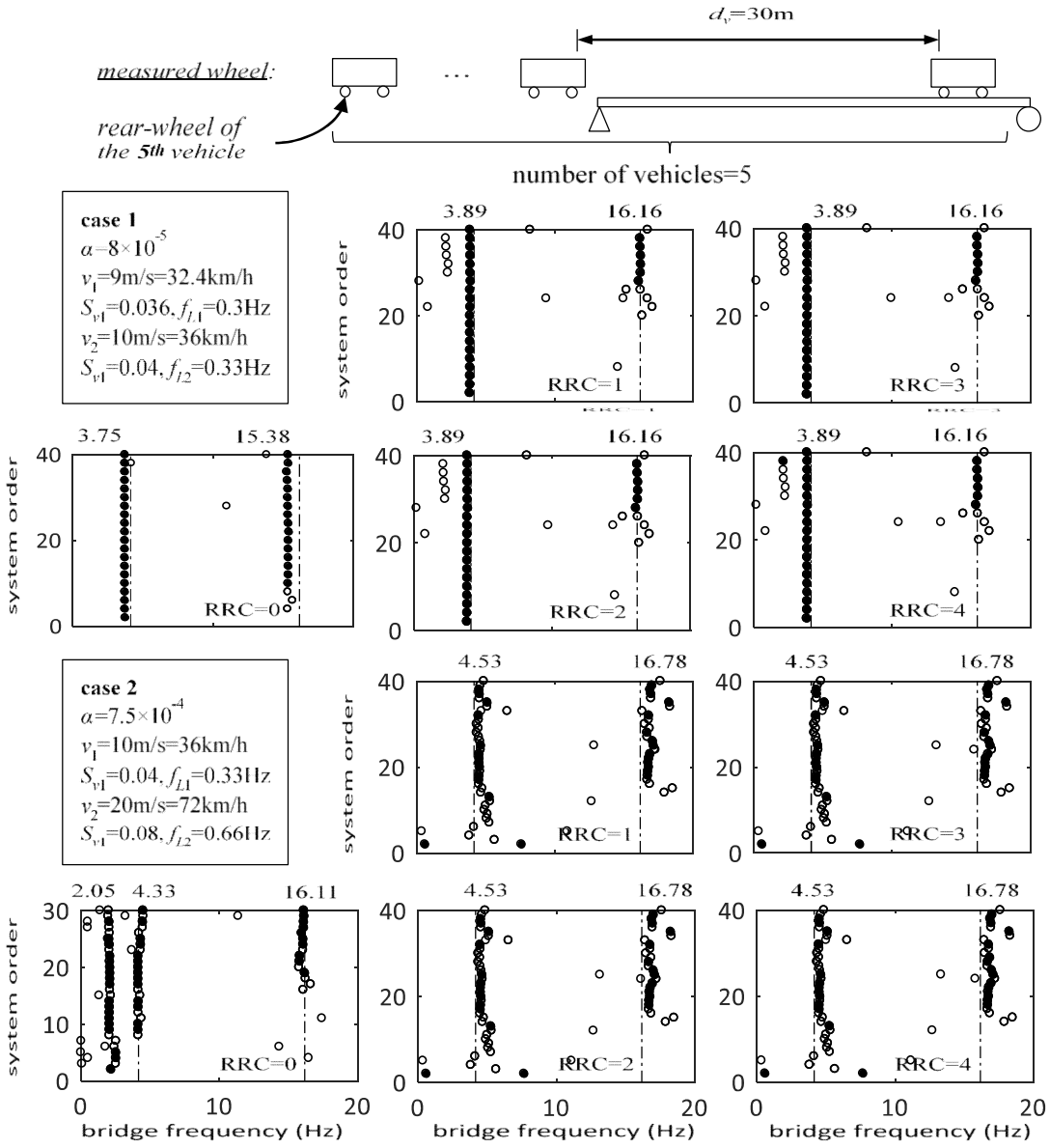

Figure 5. Stabilization diagrams for the identification results of ST-SSI for a sequence of vehicles

Table 5. Identification results of the ST-SSI method considering a sequence of vehicles

case No.	RRC	f_1^{id} (Hz)	ε_1^{id}	f_2^{id} (Hz)	ε_2^{id}	redundant frequency
1	0	3.75	9.6%	15.38	5.0%	-
	1~4	3.89	6.3%	16.16	0.2%	-
2	0	4.33	4.3%	16.11	0.5%	2.05Hz(vehicle)
	1~4	4.53	9.1%	16.78	3.6%	-

In summary, with the assistance of vehicle sequence, discussions in this section demonstrate the feasibility of identifying the bridge frequencies using a normal vehicle with practical speeds and considering RRCs simultaneously. The additional traffic enhanced the identification of bridge frequencies using measured vehicle response.

4 Conclusions

The present study offers fundamental analytical research to contribute towards an alternative indirect approach to scan bridges using test-vehicles. Conveniently, a test-vehicle may act as a portable measuring tool to identify frequencies of non-monitored bridges. In this context, the present study establishes a short-time stochastic subspace identification (ST-SSI) approach to estimate bridge frequencies by processing data from a traversing vehicle. The identification is challenging because of coupled and time-varying nature of vehicle-bridge systems.

The proposed method relies solely on the knowledge of dynamic characteristics and response of the test-vehicle, and requires no information about the bridge. The study employs a dimensionless description to deal with the time-varying nature of the VBI system, and demonstrates the feasibility and limitations of applying ST-SSI to the VBI problem. Also, the proposed approach efficiently eliminates the negative effect due to road roughness by controlling the speeds of the same vehicle for two runs. The analysis offers, for the first time to the knowledge of the authors, analytical proof of this idea for arbitrary vehicles. Crucially, this study proves it is feasible to achieve the identification of bridge frequencies via indirect identification techniques for the test-vehicle with speeds much higher (e.g., 10m/s = 36km/h and 20m/s = 72km/h) than previously considered making the proposed approach

more practical. Numerical experiments using both SDOF vehicles and a more realistic MDOF vehicle validate the proposed ST-SSI method. The SDOF vehicle can efficiently identify the first two frequencies of the examined bridge, even considering high levels of RRCs. Analyses show that a test-vehicle, with high frequency, small damping ratio and with a driving speed ratio not greater than 0.9, is preferable for the needs of the proposed approach. Focusing on the MDOF vehicle, a single vehicle is only sufficient to identify the fundamental frequency of the bridge. The identification of higher-mode frequencies requires the vehicle sequence to amplify the vibration of the bridge with higher modes.

Appendix

A.1 Order of magnitude estimation of shape functions derivative vector -

The matrix $\mathbf{W}_N^{\mathrm{B}}(\tilde{x})=\begin{bmatrix}N_1 & N_2 & N_3 & N_4\end{bmatrix}$ defines the position of the contact forces $\tilde{\lambda}_N(t)$ between the vehicle and the bridge, with the aid of the shape functions

$$N_1=1-3\frac{\Delta\tilde{x}^2}{L_e^2}+2\frac{\Delta\tilde{x}^3}{L_e^3},\ N_2=\Delta\tilde{x}\left(1-2\frac{\Delta\tilde{x}}{L_e}+\frac{\Delta\tilde{x}^2}{L_e^2}\right),\ N_3=3\frac{\Delta\tilde{x}^2}{L_e^2}-2\frac{\Delta\tilde{x}^3}{L_e^3},\ N_4=\Delta\tilde{x}\left(-\frac{\Delta\tilde{x}}{L_e}+\frac{\Delta\tilde{x}^2}{L_e^2}\right) \quad (44)$$

where L_e is the length of the element for the bridge model in forward VBI analysis which is usually smaller than 1m, $\Delta\tilde{x}\in[0,\ L_e]$ is the distance between the start point of the element and the position of contact force. The corresponding derivative term is $d\mathbf{W}_N^{\mathrm{B}}(\tilde{x})/d\tilde{x}=\begin{bmatrix}dN_1 & dN_2 & dN_3 & dN_4\end{bmatrix}/d\Delta\tilde{x}$ with the functions as

$$\frac{dN_1}{d\Delta\tilde{x}}=-6\frac{\Delta\tilde{x}}{L_e^2}+6\frac{\Delta\tilde{x}^2}{L_e^3},\frac{dN_2}{d\Delta\tilde{x}}=1-4\frac{\Delta\tilde{x}}{L_e}+3\frac{\Delta\tilde{x}^2}{L_e^2},\frac{dN_3}{d\Delta\tilde{x}}=6\frac{\Delta\tilde{x}}{L_e^2}-6\frac{\Delta\tilde{x}^2}{L_e^3},\frac{dN_4}{d\Delta\tilde{x}}=-2\frac{\Delta\tilde{x}}{L_e}+3\frac{\Delta\tilde{x}^2}{L_e^2} \quad (45)$$

This matrix with dimensionless position $x=\tilde{x}/L^{\mathrm{B}}$ is $\mathbf{W}_N^{\mathrm{B}}(x)=\mathbf{W}_N^{\mathrm{B}}(\tilde{x})$, and the differentiation term is $\mathbf{W}_N^{\mathrm{B}}(x)'=d\mathbf{W}_N^{\mathrm{B}}(x)/dx=L^{\mathrm{B}}d\mathbf{W}_N^{\mathrm{B}}(\tilde{x})/d\tilde{x}$. The order of magnitude of the matrix $\mathbf{W}_N^{\mathrm{B}}(\tilde{x})$ is approximately 1. The value of the differentiation term $d\mathbf{W}_N^{\mathrm{B}}(\tilde{x})/d\tilde{x}$ relates to the element length L_e. For instance, $dN_1/d\Delta\tilde{x}$ has the value between $-3/2L_e$ and 0. Hence, one can estimate the order of magnitude as $O\left(\mathbf{W}_N^{\mathrm{B}}(x)'\right)=O\left(L^{\mathrm{B}}d\mathbf{W}_N^{\mathrm{B}}(\tilde{x})/d\tilde{x}\right)=O\left(L^{\mathrm{B}}/L_e\right)\approx 10^2$.

A.2 Matrices in Hankel matrix

$\mathbf{X}^p$ and $\mathbf{X}^f$ are the state vectors, composed of the bridge response

$$\mathbf{X}^p = \begin{bmatrix} \Delta\mathbf{X}_1^{\mathrm{B}} & \Delta\mathbf{X}_2^{\mathrm{B}} & \cdots & \Delta\mathbf{X}_{col}^{\mathrm{B}} \end{bmatrix} \in R^{2N\times col} \tag{46}$$

$$\mathbf{X}^f = \begin{bmatrix} \Delta\mathbf{X}_{s+1}^{\mathrm{B}} & \Delta\mathbf{X}_{s+2}^{\mathrm{B}} & \cdots & \Delta\mathbf{X}_{s+col}^{\mathrm{B}} \end{bmatrix} \in R^{2N\times col}, \tag{47}$$

$\boldsymbol{\Psi}$ is the Toeplitz matrix, containing bridge properties

$$\boldsymbol{\Psi} = \begin{bmatrix} \mathbf{0} & \mathbf{0} & \mathbf{0} & \cdots & \mathbf{0} \\ \mathbf{N}^{\mathrm{V}f}\mathbf{N}_k^{\mathrm{WB}} & \mathbf{0} & \mathbf{0} & \cdots & \mathbf{0} \\ \mathbf{N}^{\mathrm{V}f}\mathbf{N}_k^{\mathrm{WB}}\mathbf{N}^{\mathrm{B}} & \mathbf{N}^{\mathrm{V}f}\mathbf{N}_k^{\mathrm{WB}} & \mathbf{0} & \cdots & \mathbf{0} \\ \vdots & \vdots & \vdots & \ddots & \vdots \\ \mathbf{N}^{\mathrm{V}f}\mathbf{N}_k^{\mathrm{WB}}\left(\mathbf{N}^{\mathrm{B}}\right)^{s-2} & \mathbf{N}^{\mathrm{V}f}\mathbf{N}_k^{\mathrm{WB}}\left(\mathbf{N}^{\mathrm{B}}\right)^{s-3} & \mathbf{N}^{\mathrm{V}f}\mathbf{N}_k^{\mathrm{WB}}\left(\mathbf{N}^{\mathrm{B}}\right)^{s-4} & \cdots & \mathbf{0} \end{bmatrix} \in R^{s\times 2Ns}, \tag{48}$$

$\mathbf{D}_N$ is the diagonal matrix including the mass matrix of the bridge

$$\mathbf{D}_N = \begin{bmatrix} \mathbf{N}^M & & \\ & \ddots & \\ & & \mathbf{N}^M \end{bmatrix} \in R^{2Ns\times 2Ns}, \tag{49}$$

$\mathbf{U}^p$ and $\mathbf{U}^f$ respectively represent the "past" and "future" Hankel matrices related to the position and magnitude of the contact force between the vehicle and the bridge, such that

$$\mathbf{U}^p = \begin{bmatrix} \mathbf{W}_{N,1}^{\mathrm{B}}\Delta\tilde{\lambda}_{N,1} & \cdots & \mathbf{W}_{N,j}^{\mathrm{B}}\Delta\tilde{\lambda}_{N,col} \\ \vdots & \ddots & \vdots \\ \mathbf{W}_{N,s}^{\mathrm{B}}\Delta\tilde{\lambda}_{N,s} & \cdots & \mathbf{W}_{N,s+col-1}^{\mathrm{B}}\Delta\tilde{\lambda}_{N,s+col-1} \end{bmatrix} \in R^{2Ns\times col} \tag{50}$$

$$\mathbf{U}^f = \begin{bmatrix} \mathbf{W}_{N,s+1}^{\mathrm{B}}\Delta\tilde{\lambda}_{N,s+1} & \cdots & \mathbf{W}_{N,s+col}^{\mathrm{B}}\Delta\tilde{\lambda}_{N,s+col} \\ \vdots & \ddots & \vdots \\ \mathbf{W}_{N,2s}^{\mathrm{B}}\Delta\tilde{\lambda}_{N,2s} & \cdots & \mathbf{W}_{N,2s+col-1}^{\mathrm{B}}\Delta\tilde{\lambda}_{N,2s+col-1} \end{bmatrix} \in R^{2Ns\times col} \tag{51}$$

A.3 Orthogonal projection using LQ decomposition

Using LQ decomposition of the Hankel matrix, one can write

$$\mathbf{H}_{\mathbf{p}}^p = \mathbf{L}_{11}\mathbf{Q}_1^{\mathrm{T}} \tag{52}$$

$$\mathbf{H}_{\mathbf{p}}^{f} = \mathbf{L}_{21}\mathbf{Q}_1^{\mathrm{T}} + \mathbf{L}_{22}\mathbf{Q}_2^{\mathrm{T}}. \tag{53}$$

According to the orthogonal projection theorem and Eqs (52) and (53), the projection of the "future" matrix $\mathbf{H}_{\mathbf{p}}^{f}$ onto the "past" matrix $\mathbf{H}_{\mathbf{p}}^{p}$ is

$$\mathrm{proj}_{\mathbf{H}_{\mathbf{p}}^{p}}\left(\mathbf{H}_{\mathbf{p}}^{f}\right) = \left(\mathbf{L}_{21}\mathbf{Q}_1^{\mathrm{T}} + \mathbf{L}_{22}\mathbf{Q}_2^{\mathrm{T}}\right)\left(\mathbf{L}_{11}\mathbf{Q}_1^{\mathrm{T}}\right)^{\mathrm{T}}\left(\mathbf{L}_{11}\mathbf{Q}_1^{\mathrm{T}}\mathbf{Q}_1\mathbf{L}_{11}^{\mathrm{T}}\right)^{-1}\mathbf{L}_{11}\mathbf{Q}_1^{\mathrm{T}} = \mathbf{L}_{21}\mathbf{Q}_1^{\mathrm{T}}\mathbf{Q}_1\mathbf{Q}_1^{\mathrm{T}} + \mathbf{L}_{22}\mathbf{Q}_2^{\mathrm{T}}\mathbf{Q}_1\mathbf{Q}_1^{\mathrm{T}} \tag{54}$$

Applying the orthogonality conditions (i.e., $\mathbf{Q}_i^{\mathrm{T}}\mathbf{Q}_j = \mathbf{I}$ for $i = j$, and $\mathbf{Q}_i^{\mathrm{T}}\mathbf{Q}_j = \mathbf{0}$ for $i \neq j$) reduces the preceding equation to

$$\mathrm{proj}_{\mathbf{H}_{\mathbf{p}}^{p}}\left(\mathbf{H}_{\mathbf{p}}^{f}\right) = \mathbf{L}_{21}\mathbf{Q}_1^{\mathrm{T}} \tag{55}$$

References

Chang, K. C., Wu, F. B., & Yang, Y. B. (2010). Effect of road surface roughness on indirect approach for measuring bridge frequencies from a passing vehicle. *IMMIJ, 3*(4), 299-308.

Chatzi, E. N., & Spiridonakos, M. D. (2015). Structural identification and monitoring based on uncertain/limited information. *MATEC Web of Conferences,*

Ferrari, R., Pioldi, F., Rizzi, E., Gentile, C., Chatzi, E. N., Serantoni, E., & Wieser, A. (2016). Fusion of wireless and non-contact technologies for the dynamic testing of a historic RC bridge. *Meas. Sci. Technol., 27*(12), 124014.

Goi, Y., & Kim, C. W. (2016). Mode identifiability of a multi-span cable-stayed bridge utilizing stabilization diagram and singular values. *Smart Struct Syst, 17*(3), 391-411.

ISO 8608. (2016). *Mechanical vibration - road surface profiles - reporting of measured data* (Second edition 2016-11-01 ed.). Geneva: ISO.

Jin, N., Paraskeva, T. S., & Dimitrakopoulos, E. G. (2017). Extraction of bridge frequencies from a passing vehicle by stochastic subspace identification. *30th KKHTCNN,* Taiwan.

Jin, N., Paraskeva, T. S., & Dimitrakopoulos, E. G. (2018). Estimation of bridge frequencies from a passing vehicle. *IABMAS2018,* Australia.

Katayama, T. (2006). *Subspace methods for system identification* Springer Science & Business Media.

Kim, C. W., Inoue, S., Sugiura, K., Mcgetrick, P., & Kawatani, M. (2016). *Extracting bridge frequencies from dynamic responses of two passing vehicles* CRC Press.

Li, J., Zhu, X., Law, S., & Samali, B. (2019). Indirect bridge modal parameters identification with one stationary and one moving sensors and stochastic subspace identification. *J. Sound Vibrat., 446*, 1-21.

Li, Y., Chen, N., Zhao, K., & Liao, H. (2012). Seismic response analysis of road vehicle-bridge system for continuous rigid frame bridges with high piers. *Earthq Eng Eng Vib, 11*(4), 593-602.

Marchesiello, S., Bedaoui, S., Garibaldi, L., & Argoul, P. (2009). Time-dependent identification of a bridge-like structure with crossing loads. *Mech Syst Signal Process, 23*(6), 2019-2028.

McGetrick, P. J., González, A., & OBrien, E. J. (2009). Theoretical investigation of the use of a moving vehicle to identify bridge dynamic parameters. *INSIGHT, 51*(8), 433-438.

Ohsumi, A., & Kawano, T. (2002). Subspace identification for a class of time-varying continuous-time stochastic systems via distribution-based approach. *IFAC Proceedings Volumes, 35*(1), 241-246.

Paraskeva, T. S., Dimitrakopoulos, E. G., & Zeng, Q. (2017). Dynamic vehicle–bridge interaction under simultaneous vertical earthquake excitation. *B. Earthq. Eng., 15*(1), 71-95.

Siringoringo, D. M., & Fujino, Y. (2012). Estimating bridge fundamental frequency from vibration response of instrumented passing vehicle: Analytical and experimental study. *Adv. Struct. Eng., 15*(3), 417-433.

Stoura, C. D., & Dimitrakopoulos, E. G. (2019). A rational method to decouple the train-bridge interaction problem. *COMPDYN 2019,* Greece.

Stoura, C. D., & Dimitrakopoulos, E. G. (2020). Additional damping effect on bridges because of vehicle-bridge interaction. *J.Sound Vibrat.,* 115294.
Stoura, C. D., & Dimitrakopoulos, E. G. (accepted on14 Apr 2020, in press). A modified bridge system method to characterize and decouple vehicle-bridge interaction. *Acta Mechanica.*
Urushadze, S., & Yau, J. (2017). Experimental verification of indirect bridge frequency measurement using a passing vehicle. *Procedia Engineering, 190*, 554-559.
Van Overschee, P., & De Moor, B. L. (2012). *Subspace identification for linear systems: Theory—Implementation—Applications* Springer Science & Business Media.
Yang, J. P., & Lee, W. (2018). Damping effect of a passing vehicle for indirectly measuring bridge frequencies by EMD technique. *Int. J. Str. Stab. Dyn, 18*(01), 1850008.
Yang, Y. B., Chen, W. F., Yu, H. W., & Chan, C. S. (2013a). Experimental study of a hand-drawn cart for measuring the bridge frequencies. *Eng.Struct., 57*, 222-231.
Yang, Y. B., Lin, C. W., & Yau, J. D. (2004a). Extracting bridge frequencies from the dynamic response of a passing vehicle. *J. Sound Vibrat., 272*(3), 471-493.
Yang, Y. B., Xu, H., Zhang, B., Xiong, F., & Wang, Z. L. (2020). Measuring bridge frequencies by a test vehicle in non-moving and moving states. *Eng.Struct., 203*, 109859.
Yang, Y. B., & Yang, J. P. (2018). State-of-the-art review on modal identification and damage detection of bridges by moving test vehicles. *Int. J. Str. Stab. Dyn, 18*(2), 1850025.
Yang, Y. B., & Yau, J. D. (2017). Resonance of high-speed trains moving over a series of simple or continuous beams with non-ballasted tracks. *Eng.Struct., 143*, 295-305.
Yang, Y. B., Yau, J. D., Yao, Z., & Wu, Y. S. (2004b). *Vehicle-bridge interaction dynamics: With applications to high-speed railways* World Scientific.
Yang, Y. B., & Chang, K. C. (2009). Extracting the bridge frequencies indirectly from a passing vehicle: Parametric study. *Eng. Struct., 31*(10), 2448-2459.
Yang, Y. B., Chang, K. C., & Li, Y. C. (2013b). Filtering techniques for extracting bridge frequencies from a test vehicle moving over the bridge. *Eng. Struct., 48*, 353-362.
Yang, Y. B., & Chen, W. (2015). Extraction of bridge frequencies from a moving test vehicle by stochastic subspace identification. *J. Bridge Eng., 21*(3), 4015053.
Yang, Y. B., Cheng, M. C., & Chang, K. C. (2013c). Frequency variation in vehicle–bridge interaction systems. *International Journal of Structural Stability and Dynamics, 13*(2), 1350019.
Yang, Y. B., Li, Y., & Chang, K. (2012). Using two connected vehicles to measure the frequencies of bridges with rough surface: A theoretical study. *Acta Mech, 223*(8), 1851-1861.
Zeng, Q., Yang, Y. B., & Dimitrakopoulos, E. G. (2016). Dynamic response of high speed vehicles and sustaining curved bridges under conditions of resonance. *Eng.Struct., 114*, 61-74.